Articles

Contribution from the Departamento de Química Inorgánica, Universidad del País Vasco, Apartado 644, 48080 Bilbao, Spain, Departament de Química Inorgánica (UIBCM), Universitat de Valencia, Dr. Moliner 50, 46100 Burjassot, Valencia, Spain, and Fachbereich Chemie, Universität Marburg, Hans-Meerwein-Strasse, D-3550 Marburg, West Germany

Fluxionality in Hexacoordinated Copper(II) Complexes with 2,2′:6′,2″-Terpyridine (terpy) and Related Ligands: Structural and Spectroscopic Investigations

José-Vicente Folgado,*,† Wolfgang Henke,‡ Rudolf Allmann,‡ Horst Stratemeier,‡,§ Daniel Beltrán-Porter,† Teófilo Rojo,∥ and Dirk Reinen*,‡

Received September 8, 1989

Variable-temperature EPR spectra of $Cu(terpy)_2(PF_6)_2$ (terpy = 2,2′:6′,2″-terpyridine) revealed that the low-temperature structure contains elongated CuN_6 octahedra with an orthorhombic component as a consequence of the Jahn–Teller effect and rigid ligand strain. The high-temperature phase is characterized by compressed octahedra in the time average (planar dynamics). Structural relations between the various low-temperature phases of compounds $Cu(terpy)_2X_2 \cdot nH_2O$ (X = NO_3, ClO_4, PF_6, Br) with respect to the cooperative Jahn–Teller order patterns are given, and the structure for the complex with X = Br and n = 3 is reported (298 K). It is triclinic, space group $P\bar{1}$, with a = 19.763 (4) Å, b = 9.563 (2) Å, c = 8.537 (1) Å, α = 95.96 (1)°, β = 93.48 (1)°, γ = 94.44 (1)°, and Z = 2. The least-squares refinement of the structure leads to an R factor of 0.068. Complexes $Cu(tpt)_2X_2 \cdot nH_2O$ [tpt = 2,4,6-tris(2-pyridyl)-1,3,5-triazine; X = NO_3, BF_4, ClO_4, n = 1; X = PF_6, n = 3] and the compound $Cu(bpca)_2 \cdot H_2O$ [bpca = *N*-(2-pyridylcarbonyl)-2-pyridinecarboximidate] were characterized by variable-temperature EPR spectroscopy. As for terpy as the ligand, the molecular CuN_6 geometry is determined by the vibronic Jahn–Teller coupling and a compression due to the rigid ligand. This model yields a structure of the ground-state potential surface that readily explains the dynamic features with increasing temperature. Finally, bonding parameters have been extracted from the copper hyperfine structures in the EPR signals, which are nicely resolved in some of the pure compounds and in the Cu^{2+}-doped Zn^{2+} complexes, which have also been prepared.

Introduction

The σ-antibonding ^2E_g ground state of Cu^{2+} ions in octahedral ligand fields is strongly Jahn–Teller unstable. A pronounced distortion of the ligand environment and a considerable splitting of the ground state are induced by the $E_g \times \epsilon_g$ vibronic coupling, where ϵ_g is the Jahn–Teller active vibrational mode (Figure 1). The resulting ground-state potential surface (Figure 1) has minima at rather large values of the radial distortion parameter ρ, which is defined as follows:

$$\rho = [2(\Delta a_x^2 + \Delta a_y^2 + \Delta a_z^2)]^{1/2} \quad (1)$$

The Δa_i values ($i = x, y, z$) are the deviations of the copper–ligand spacings from the averaged distance of the undistorted octahedron. Though any D_{2h} or D_{4h} symmetry corresponding to a linear combination of Q_θ and Q_ϵ may be stabilized, flat minima along the direction 0, 120, and 240° for the angular parameter φ indicate a preference for D_{4h} geometries, which are elongated along the molecular z, y, and x axes. If the octahedron is subject to strain effects, the potential surface distorts.[1-3] In complexes of the type $M(terpy)_2^{2+}$, the predominant strain component of the rigid terpyridine ligand corresponds to a distinct compression along the molecular z axis of the MN_6 polyedron (Figure 2). This is nicely documented by the Ni^{2+} compounds (see below), because the $^3A_{2g}$ ground state of octahedral Ni^{2+} is Jahn–Teller stable and the NiN_6 geometry solely reflects the strain effects imposed by the ligands and/or steric packing effects in the unit cell. The rigid ligand strain acts along the φ = 180° direction and lowers the two minima at 120 and 240° with respect to the one at 0°, shifting them to (orthorhombic) values φ = 120° + δ and 240° − δ ($\delta > 0$°) (Figure 1). If the height of the saddlepoint at 180° is in the range of thermal energies, it is expected that at high temperatures vibrational levels above the saddlepoint are occupied and a tetragonally compressed CuN_6 polyhedron results as a dynamically averaged geometry. At lower temperatures the system is localized in either minimum with equal probability, with the long Cu–N spacings of the orthorhombically distorted CuN_6 polyhedron ($a_z < a_{y(x)} < a_{x(y)}$; see eq 1) extending alternatively along the molecular x and y axes (Figure 2).

Additionally the ground-state potential surface may be influenced by strains due to the elastic interactions between the distorted CuN_6 polyhedra (cooperative Jahn–Teller effect). The elastic coupling is small, however, if the polyhedra are isolated from each other in the unit cell. In case of an antiferrodistortive order[3] two sublattices exist, the long axes of which have a perpendicular orientation with respect to each other. The corresponding strain has the same symmetry as the one imposed on the system by the rigid ligand. While the antiferrodistortive order determines the low-temperature phase, a high-temperature phase with time-averaged compressed octahedra [$a_\parallel \approx a_z$; $a_\perp \approx {}^1/_2(a_x + a_y)$] is expected to exist ("planar dynamics"),[3] which is characterized by a tetragonal **g** tensor (see below). If the strains are strong enough, a thermal population of the φ = 0° minimum is not possible. The alternative ferrodistortive order with the long axes of the polyhedra in parallel orientation will energetically slightly favor one of the two lower minima with respect to the other. A planar dynamics in the strict sense is not expected in this case, because an equal distribution over both minima is only expected at rather high temperatures. The proposed models, which have been quantitatively applied to various octahedral Cu^{2+} systems,[3] are also suitable to explain the main structural features of $Cu(terpy)_2X_2 \cdot nH_2O$ compounds, as will be shown below.

For the sake of comparison with the terpyridine ligand, we have also investigated the compounds $Cu(tpt)_2X_2 \cdot nH_2O$ and $Cu(bpca)_2 \cdot H_2O$, where "tpt" [2,4,6-tris(2-pyridyl)-1,3,5-triazine] and "bpca" [*N*-(2-pyridylcarbonyl)-2-pyridinecarboximidate] are re-

† Universitat de Valencia.
‡ Universität Marburg.
§ Present address: University of Tasmania, Hobart, TAS 7001, Australia.
∥ Universidad del País Vasco.

(1) Reinen, D.; Krause, S. *Inorg. Chem.* **1981**, *20*, 2750.
(2) Riley, M. J.; Hitchman, M. A.; Reinen, D.; Steffen, G. *Inorg. Chem.* **1988**, *27*, 1924.
(3) Reinen, D.; Friebel, C. *Struct. Bonding (Berlin)* **1979**, *37*, 1.

0020-1669/90/1329-2035$02.50/0

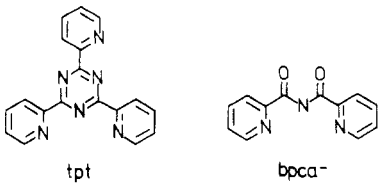

lated N-donor tridentate rigid quasiplanar ligands. Although Cu^{2+} promotes hydrolysis of tpt, and Cu(II)–bpca derivatives are usually obtained,[4,5] we have been able to isolate the $Cu(tpt)X_2 \cdot nH_2O$ compounds recently[4] and are reporting here the synthesis and characterization of the $Cu(tpt)_2X_2 \cdot nH_2O$ derivatives.

Finally, we have derived information about the nature of the Cu(II) ground-state wave function from the **g** tensors and the hyperfine structure, which is nicely resolved in the EPR spectra of some of the pure compounds and in those of Cu^{2+}-doped Zn^{2+} complexes.

Experimental Section

Preparation of the Compounds. Complexes of the type $Cu(terpy)_2X_2 \cdot nH_2O$ were first prepared by Morgan and Burstall.[6] terpy is dissolved in hot water, the metal salt is added, and the solution is evaporated until the complexes crystallize. The water content of these complexes varies in dependence on the preparation and drying conditions. In some cases (see below) a variation in the number of H_2O molecules is critical, because the structure may change. Dark green crystal needles of $Cu(terpy)_2Br_2 \cdot 3H_2O$ were obtained by cooling a saturated solution from 35 to 15 °C with a gradient of 0.03 °C h^{-1}. The complexes $Cu(terpy)_2(PF_6)_2$ and $Cu(bpca)_2 \cdot H_2O$, as well as the analogous Cu(II)-doped Zn(II) compounds, were prepared in a similar way as previously described.[7,8] The complexes $Cu(tpt)_2X_2 \cdot H_2O$ ($X = NO_3$, BF_4, ClO_4) were prepared by mixing the corresponding copper(II) salt and the ligand, in molar ratio 1:2, dissolved in the minimum amount of ethanol. The pale green powders obtained were separated from the solution by filtration, washed with cold ethanol, and dried in a desiccator over silica gel. The complex $Cu(tpt)_2(PF_6)_2 \cdot 3H_2O$ was prepared in the following way: $Cu(NO_3)_2 \cdot 3H_2O$ dissolved in ethanol (1 mmol/20 mL) was added to an ethanolic solution of tpt (2 mmol/60 mL) with stirring, and no precipitate was observed. To the green solution was added with stirring KPF_6 dissolved in acetone (10 mmol/15 mL), and a fine powder immediately appeared, which was separated and stored as above. Powder samples of $Cu_\epsilon Zn_{1-\epsilon}(tpt)_2X_2 \cdot nH_2O$, with $\epsilon \leq 0.05$, were also prepared in the way described above, but starting from the appropriate amounts of the corresponding Cu(II) and Zn(II) salts. The analytical data are listed in Table I.

Physical Measurements. Infrared spectra were obtained with KBr pellets in the 4000–250-cm^{-1} region by using a Pye-Unicam SP 2000 spectrophotometer. Diffuse-reflectance electronic spectra were recorded on Perkin-Elmer Lambda 9 UV/vis/near-IR and Zeiss PMQII spectrophotometers. EPR spectra were recorded on a Varian E15 spectrometer at 35 GHz, in the temperature range 4.2–300 K. Water was thermogravimetrically determined with a Setaram B70 simultaneous TGA–DTA thermobalance. X-ray powder diffraction patterns ($5 \leq 2\theta \leq 50°$) were performed on a Kristalloflex 810 Siemens diffractometer, using Cu Kα radiation and silicon powder as internal reference.

X-ray Structure Determination of $Cu(terpy)_2Br_2 \cdot 3H_2O$. A single crystal (1.1 × 0.4 × 0.2 mm) was sealed into a glass tube together with a drop of mother liquid, in order to avoid a loss of water (see below), mounted on a Philips PW 1100 automatic diffractometer, and used for data collection. Details on crystal data, intensity collection, and refinement are listed in Table II. The intensities of three standard reflections measured every 90 min did not show any systematic variation. Corrections for the background, as well as for Lorentz and polarization effects, were applied, but not for absorption. Because the compound is isostructural with $Co(terpy)_2Br_2 \cdot 3H_2O$,[9] we used the atomic positions of the latter complex, with the exception of H_2O and Br, as starting parameters.

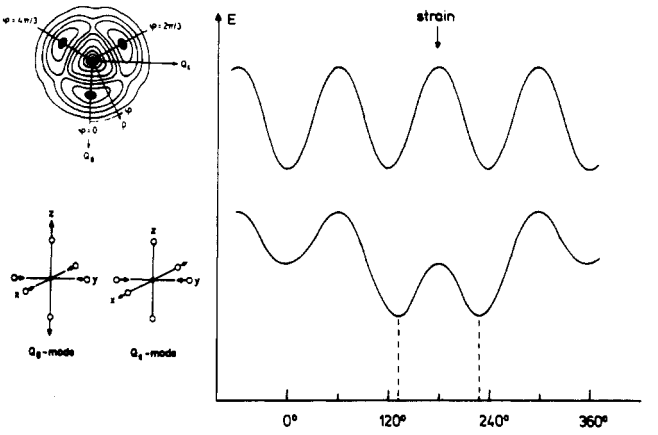

Figure 1. Vibrational ϵ_g modes (Q_θ, Q_ϵ) and warping in the lower potential surface by nonlinear Jahn–Teller coupling (left) and circular cross section along the angular coordinate at $\rho = \rho_{min}$ (right) in the absence (above) and in the presence of strain (compression along z) (below).

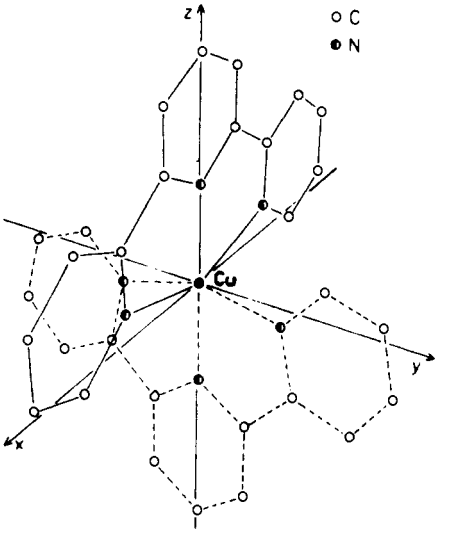

Figure 2. Geometry of $Cu(terpy)_2^{2+}$ polyhedra.

During the refinement procedures it was found that, as for the Co^{2+} compound, one of the Br atoms was statistically distributed between two positions. The same is true for one of the three H_2O molecules. The final refinement in the X-RAY 72 system[10] with the full matrix led to a reliability index of $R = 0.146$. Because of the large number of parameters (478), the anisotropic refinement was continued in the block-diagonal program of Ahmed,[10] yielding an R value of 0.068. The positions of the H atoms of the terpy rings were calculated on the basis of the rigid ligand geometry and the assumption d(C–H) = 1 Å and ∠C–C–H = 120°. The occupation numbers for the two positions of one Br atom were 0.384 (6) and 0.545 (5) whereas those for the disordered water molecule were fixed at 0.4 and 0.6. The final R value is based on 2517 independent reflections, because 956 reflections were considered as unobserved with $F < 2\sigma(F)$. In the last refinement 324 reflections of the latter group of 956 were calculated to have F values between 2- and 3$\sigma(F)$. The least-squares calculations in the X-RAY 72 system were based on the complete set of 3473 reflections, however. The positional parameters and temperature factors are collected in Table III. The interatomic distances and bond angles are given in Figure 3, and the unit cell is depicted in Figure 4.

The complex $Cu(terpy)_2Br_2 \cdot nH_2O$ ($n = 3$) loses water when exposed to air for long periods of time, which changes the structure. From Simon–Guinier diagrams of powder samples, which are treated with a N_2 flow of 50 °C, a sharp phase transition from the triclinic unit cell ($n = 3$), with dimensions as given in Table II, to a tetragonal structure with $a = 12.48$ (1) Å and $c = 36.8$ (2) Å is observed. It occurs, after a shrinking process of the triclinic cell particularly in the a direction, at

(4) Folgado, J. V.; Escrivá, E.; Beltrán-Porter, A.; Beltrán-Porter, D. *Transition Met. Chem. (Weinheim, Ger.)* **1986**, *11*, 485; **1987**, *12*, 306.
(5) Folgado, J. V.; Coronado, E.; Beltrán-Porter, D.; Burriel, R.; Fuertes, A.; Miravitlles, C. *J. Chem. Soc., Dalton Trans.* **1988**, 3041.
(6) Morgan, G.; Burstall, F. M. *J. Chem. Soc.* **1937**, 1655.
(7) Arriortua, M. I.; Rojo, T.; Amigó, J. M.; Germain, G.; Declercq, J. P. *Acta Crystallogr., Sect. B.: Struct. Crystallogr. Cryst. Chem.* **1982**, *B38*, 1323.
(8) Marcos, D.; Martínez-Mañez, R.; Folgado, J. V.; Beltrán-Porter, A.; Beltrán-Porter, D.; Fuertes, A. *Inorg. Chim. Acta* **1989**, *159*, 11.
(9) Maslen, E. N.; Raston, C. L.; White, A. H. *J. Chem. Soc., Dalton Trans.* **1974**, 1803.
(10) (a) Stewart, J. M.; Kundell, F. A.; Baldwin, J. C. *X-Ray 72 Systems of Crystallographic Programs*; University of Maryland: College Park, Md, 1970. (b) Ahmed, F. R.; Hall, R. S.; Pippy, M. E.; Haber, C. P. *BLOCDIAG. Wordlist of Crystallographic Programs*, 2nd ed.; Munksgaard International Book Sellers and Publishers, Ltd.: Copenhagen, 1976; App. 52.

Table I. Analytical and Electronic Spectroscopic Data

compd	% found (% calc)			unit cell dimens, Å			ligand field data (298 K)	
	C	N	H	*a*	*b*	*c*	Δ_0, cm^{-1} [a]	$^4E_{JT}$, cm^{-1} [b]
$Cu(tpt)_2(NO_3)_2 \cdot H_2O$	51.8 (52.1)	23.3 (23.6)	2.9 (3.1)	8.01 (1)	8.01 (1)	19.1 (1)	10300	6600
$Cu(tpt)_2(BF_4)_2 \cdot H_2O$	49.1 (49.1)	18.9 (19.1)	2.9 (3.0)	8.04 (4)	8.04 (4)	19.1 (1)	10100	6800
$Cu(tpt)_2(ClO_4)_2 \cdot H_2O$	47.5 (47.8)	18.7 (18.6)	2.7 (2.9)	8.04 (4)	8.04 (4)	19.1 (1)	10050	6900
$Cu(tpt)_2(PF_6)_2 \cdot 3H_2O$	42.0 (41.9)	16.5 (16.3)	2.8 (2.9)	7.87 (1)	8.44 (1)	22.3 (1)	10500	6200
$Cu(terpy)_2Br_2 \cdot 3H_2O$	48.1 (48.4)	11.3 (11.3)	3.2 (3.8)				11250	6100

[a] Difference between the averaged $d_{z^2-y^2}$, d_{x^2} and d_{yz}, d_{xz}, d_{xy} energies, respectively. [b] ^2E ($d_{z^2-y^2}$, d_{x^2}) ground-state splitting.

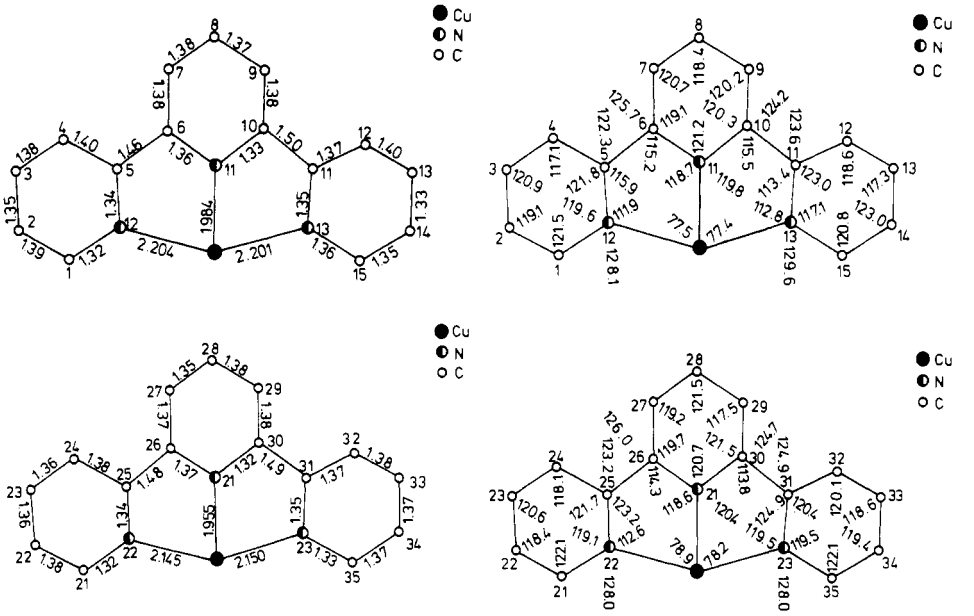

Figure 3. Interatomic distances (Å, left) and bond angles (deg, right) in $Cu(terpy)_2Br_2 \cdot 3H_2O$. Standard deviations: σ(Cu–N) = 0.009 Å; σ(C–C) = σ(C–N) = 0.01 Å; σ(N–Cu–N) = σ(C–C(N)–C) = 0.9°.

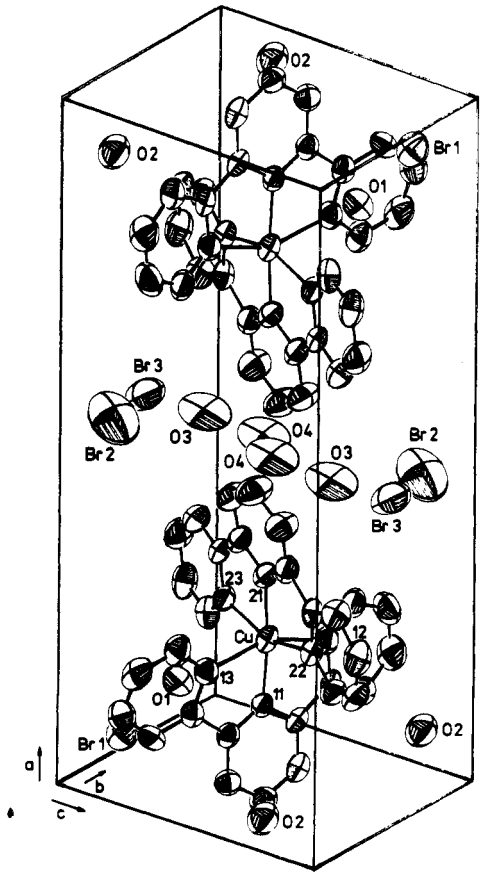

Figure 4. Perspective view of the unit cell of $Cu(terpy)_2Br_2 \cdot 3H_2O$ and atomic numbering.

Table II. Crystallographic Data for $Cu(terpy)_2Br_2 \cdot 3H_2O$

formula $C_{30}H_{28}N_6O_3CuBr_2$	fw = 743.34
a = 19.763 (4) Å	Z = 2
b = 9.563 (2) Å	space group $P\bar{1}$
c = 8.537 (1) Å	T = 20 °C
α = 95.96 (1)°	λ = 0.7107 Å
β = 93.48 (1)°	ρ_{calcd} = 1.53 g cm^{-3}
γ = 94.44 (1)°	μ = 20.84 cm^{-1}
V = 1614 (1) Å^3	$R(F_o)$ = 0.068
	$R_w(F_o)$ = 0.069

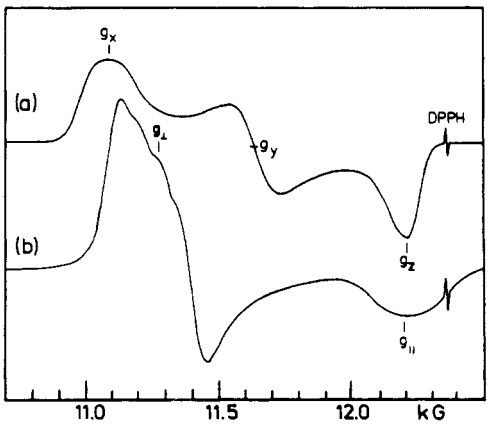

Figure 5. EPR powder spectra (35 GHz) of $Cu(terpy)_2(PF_6)_2$ at 4.2 K (a) and room temperature (b).

$n \approx 1$. The final lattice parameters, which necessarily refer to the compound with n = 0, are a = 12.32 (1) Å and c = 36.1 (2) Å. The tetragonal structure is closely related to the one of $Cu(terpy)_2(NO_3)_2$[11] and will be discussed below.

(11) Allmann, R.; Henke, W.; Reinen, D. *Inorg. Chem.* **1978**, *17*, 378.

Table III. Atomic Parameters for $Cu(terpy)_2Br_2 \cdot 3H_2O$[a]

atom	x	y	z	σ	B	atom	x	y	z	σ	B
Cu	0.7541	0.6418	0.4116	1	3.82 (5)						
N11	0.8539	0.6492	0.4208	7	3.6 (4)	N21	0.6570	0.6544	0.4120	8	4.3 (4)
N12	0.7703	0.4301	0.3085	7	4.2 (4)	N22	0.7326	0.7233	0.1886	7	4.0 (4)
N13	0.7860	0.8578	0.5152	7	4.3 (4)	N23	0.7327	0.5582	0.6303	7	4.2 (4)
C1	0.7250	0.3208	0.2710	10	5.0 (5)	C21	0.7752	0.7559	0.0831	10	4.8 (5)
C2	0.7439	0.1895	0.2223	12	6.3 (7)	C22	0.7563	0.8238	−0.0471	11	5.7 (6)
C3	0.8102	0.1734	0.2126	12	6.6 (7)	C23	0.6911	0.8539	−0.0684	11	6.2 (6)
C4	0.8584	0.2844	0.2526	10	5.0 (5)	C24	0.6458	0.8180	0.0367	11	5.4 (6)
C5	0.8359	0.4138	0.3026	9	3.8 (4)	C25	0.6686	0.7541	0.1670	9	4.0 (5)
C6	0.8823	0.5383	0.3522	9	3.7 (4)	C26	0.6250	0.7152	0.2922	10	4.5 (5)
C7	0.9508	0.5495	0.3396	10	4.7 (5)	C27	0.5587	0.7395	0.2992	12	6.6 (7)
C8	0.9906	0.6698	0.4004	10	5.0 (5)	C28	0.5268	0.7064	0.4271	13	7.5 (7)
C9	0.9605	0.7773	0.4737	10	4.6 (5)	C29	0.5584	0.6443	0.5476	12	6.4 (6)
C10	0.8914	0.7665	0.4803	9	3.8 (4)	C30	0.6247	0.6193	0.5347	10	4.5 (5)
C11	0.8532	0.8817	0.5497	9	3.9 (5)	C31	0.6666	0.5528	0.6534	9	4.0 (5)
C12	0.8836	1.0021	0.6336	10	5.2 (5)	C32	0.6427	0.4927	0.7810	11	5.8 (6)
C13	0.8432	1.1050	0.6863	12	6.0 (6)	C33	0.6859	0.4334	0.8833	12	6.3 (6)
C14	0.7772	1.0809	0.6472	12	6.4 (6)	C34	0.7523	0.4380	0.8566	11	5.7 (6)
C15	0.7481	0.9605	0.5651	10	5.3 (6)	C35	0.7743	0.5014	0.7292	10	5.1 (5)
O1	0.9147	0.3904	0.9089	8	6.5 (4)	Br1	0.9491	0.7319	0.9115	1	6.77 (7)
O2	0.9496	0.0007	0.1994	8	7.3 (5)	Br2	0.5405	0.1333	0.1231	7	15.4 (5)
O3	0.6047	0.0904	0.5024	30	15 (2)	Br3	0.5424	0.3586	0.1071	3	11.2 (2)
O4	0.5794	0.0687	0.7820	23	19 (2)						

[a] One Br and one H_2O position are split with the following occupation factors: Br2 = 0.384 (6), Br3 = 0.545 (5), H_2O3 = 0.4 (fixed), H_2O4 = 0.6 (fixed). σ is the averaged absolute positional standard deviation (in 10^3Å) = $(\sigma(x)a + \sigma(y)b + \sigma(z)c)/3$. B is the averaged temperature factor = $(B_{11} + B_{22} + B_{33})/3$ (in Å^2).

Table IV. Relevant Structural and Spectroscopic Data for $Cu(terpy)_2X_2 \cdot nH_2O$ and Related Compounds[a]

compd	space group	a_z, Å	a_y, Å	a_x, Å	$\bar{a}$, Å	ρ, Å	φ, deg	$4E_{JT}$, 10^3 cm^{-1}	T, K	ref
$Ni(terpy)_2(NO_3)_2 \cdot 3H_2O$	$P4_2/n$[b]	2.002 (8)	$=a_x$	2.128 (8)	2.089	0.14_5	180		298	12
$Co(terpy)_2I_2 \cdot 2H_2O$	$P4_2/n$	1.942 (7)	$=a_x$	2.104 (5)	2.050	0.18_5	180		298	13
	$P4_2/n$	1.912 (7)	$=a_x$	2.083 (4)	2.026	0.21	180		120	13
	$(I4_1/a)$				≃2.03	*0.26*	*158*	≃7.5	4.2	14
$Cu(terpy)_2(NO_3)_2$	$I4_1/a$	1.99[c]	2.085 (4)	2.288 (4)	2.121	0.31	136	6.5_5	298	11
	$I4_1/a$	≃1.99	≃2.05	≃2.32	≃2.12	*0.35_5*	*130*	7.3_5	<77	15
$Cu(terpy)_2(PF_6)_2$	$P\bar{4}2_1c$	1.977 (8)	$=a_x$	2.179 (7)	2.112	0.23_5	180	6.0	298	7
	$(I\bar{4})$	≃1.98	≃2.10	≃2.26	≃2.11	*≃0.28*	*≃146*	6.1	4.2	this work
$Cu(terpy)_2X_2 \cdot H_2O$ (X = ClO_4, Br)						*≃0.30*	*≃139*	6.1	4.2	15
$Cu(terpy)_2Br_2 \cdot 3H_2O$	$P\bar{1}$	1.97 (1)	2.15 (1)	2.20 (1)	2.11	0.24	165	6.1	298	this work
	$P\bar{1}$	≃1.97	≃2.11	≃2.24	≃2.11	≃0.27	150	6.1	170	this work
$Co(terpy)_2Br_2 \cdot 3H_2O$	$P\bar{1}$	1.88 (1)	$=a_x$	2.10 (2)	2.03	0.24	180		298	9
$Cu(bpca)_2 \cdot H_2O$[d]	$P2_1/c$	1.98 (2)	2.091 (6)	2.299 (6)	2.123	0.32_5	143	7.8	298	8
	$P2_1/c$	1.98	2.06	2.33	2.12	*0.36_5*	*133*		4.2	this work

[a] Presumable space groups, derived from EPR single-crystal data, are given in parentheses. The italicized values correspond to the static limits. The ρ values for the low-temperature phases of Cu(II) complexes have been calculated from the φ values, assuming a_z and $\bar{a}$ to be constant. [b] Only the substructure could be solved (see text and ref 12). [c] Average value between 1.965 (5) and 2.012 (5) Å. [d] Monoclinic, β = 95.49 (2)°.

Results and Discussion

Structure of the Low-Temperature Phase of $Cu(terpy)_2(PF_6)_2$. $Cu(terpy)_2(PF_6)_2$ crystallizes at 298 K in the tetragonal space group $P\bar{4}2_1c$ (Table IV), the CuN_6 entities having compressed octahedral geometry with the shortest Cu–N bonds perpendicular to the (001) plane.[7] In agreement with the compressed geometry of the CuN_6 octahedra, the 298 K EPR powder spectrum is of "inverse" axial type, with $g_\perp > g_\parallel > 2.00_2$ (Figure 5b), and only one signal is observed in the single-crystal EPR experiment. There is no angular dependence in the (001) plane, within the experimental error, but a well-resolved hyperfine structure is observed in some orientations. While the EPR powder spectra remain practically the same down to about 77 K, the **g** tensor becomes orthorhombic below this temperature (Figure 5a). A similar behavior of the **g** tensor with decreasing temperature has been reported for $Cu(terpy)_2X_2 \cdot H_2O$ (X = ClO_4, Br)[11,15] and can be explained in terms of a "planar-dynamic" process, which freezes in and induces a phase transition at low temperatures (see Introduction). The thermally averaged Cu–N bond lengths in the (001) plane become inequivalent; two spacings increase while the other two approach the shortest distances along [001]. Moreover, the low-temperature cooperative order we propose for this complex is that depicted in Figure 6a. Such an arrangement of the CuN_6 polyhedra is supported by several experimental facts. While one signal is observed in the (001) plane in the EPR single-crystal spectrum at 298 K, there are four signals in the 4.2 K spectrum. Because the angular dependence in the low-temperature phase cannot be easily followed due to the superimposition of the rather broad signals, we have recorded the EPR powder and single-crystal spectra of Cu^{2+} ions doped into $Zn(terpy)_2(PF_6)_2$ samples. The structure of the Zn^{2+} salt is unknown, but from the X-ray powder diffraction patterns it can be derived that it crystallizes with the same tetragonal unit cell as the Cu^{2+} compound. The EPR single-crystal data are completely analogous to those of the pure Cu^{2+} compound. The angular dependencies in the (001) and (100) [or (010)] planes are depicted in Figure 7 for 298 and 4.2 K. In the doped compound well-resolved hyperfine structure is observed in the g_z and g_x signals. At 77 K the single signal in the (00$\bar{1}$) plane is already slightly split, in correspondence to the situation for the Cu^{2+} compound itself. A continuous phase transition with a critical temperature above 77 K seems to occur (see below). The angular dependence of the **g** tensor at 4.2 K fully agrees with the existence

(12) Henke, W. Ph.D. Thesis, Marburg, FRG, 1980.
(13) Figgis, B. N.; Kucharski, E. S.; White, A. H. *Aust. J. Chem.* **1983**, *36*, 1527.
(14) Kremer, S.; Henke, W.; Reinen, D. *Inorg. Chem.* **1982**, *21*, 3013.
(15) Henke, W.; Reinen, D. Z. *Anorg. Allg. Chem.* **1977**, *436*, 187.

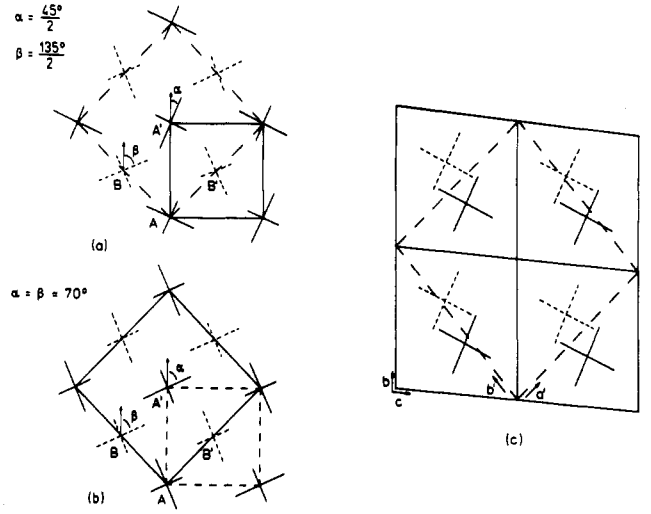

Figure 6. Projection of CuN_6 chromophores onto the (001) plane for the proposed low-temperature phase of $Cu(terpy)_2(PF_6)_2$ (a) and for the room-temperature phase of $Cu(terpy)_2(NO_3)_2$ (b), as well as onto the (100) plane of the triclinic unit cell of $Cu(terpy)_2Br_2 \cdot 3H_2O$ (c): full lines, unit cell dimensions at 298 K; broken lines, low-temperature and hypothetical high-temperature phases in (a) and (b), respectively. In (c) the structural relation with the unit cell of the nitrate at 298 K (broken lines) is shown.

of four sublattices of elongated CuN_6 octahedra in the unit cell, which are antiferrodistortively ordered in a two by two manner. The longest Cu–N axes of the four magnetically inequivalent polyhedra, which are correlated with the molecular g_x component, make angles of ≈45 and 90° between each other and angles of ±45°/2 and ±135°/2 with respect to the a axis. In case of dynamical averaging in the (001) plane, two sublattices would remain, with an orientation of the equatorial Cu–N spacings of ±45°/2 toward a, in excellent agreement with the 298 K structure and clearly within the experimental adjusting error of ±5°. The structural implications of these spectroscopic results are discussed more thoroughly in the next section.

High- and Low-Temperature Structures of Complexes $Cu(terpy)_2X_2 \cdot nH_2O$. $Cu(terpy)_2(NO_3)_2$ crystallizes in the space group $I4_1/a$.[11] From the eight Cu^{2+} entities in the unit cell, which occupy the 8e position on a 2-fold axis parallel to c with the coordinates 0, 0, z [z = –0.235 26 (2), origin at $\bar{4}$], only two are magnetically inequivalent.[15] They constitute an antiferrodistortive order between the long and intermediate Cu–N bond lengths of the CuN_6 entities in the (001) plane, while the short Cu–N spacings are oriented in the [001] direction (Table IV, Figure 6b). For the high-temperature phase, which cannot be observed below the decomposition temperature in this case (but see below), a dynamic averaging of the Cu–N bond lengths in the (001) plane is expected, leading to a reduced unit cell size ($a' = a/\sqrt{2}$; $c' = c/2$) with the space group $P4_2/n$ and $Z = 2$. It results from $I4_1/a$ with $z = -1/4$, which introduces a $\bar{4}$ axis for the CuN_6 entities (2b position in $P4_2/n$, origin at $\bar{4}$). The matrix (M1) transforms the coordinates of the

$$\begin{pmatrix} 1 & 1 & 0 \\ -1 & 1 & 0 \\ 0 & 0 & 2 \end{pmatrix} \qquad \text{(M1)}$$

$I4_1/a$ into those of the $P4_2/n$ unit cell. The space group $P4_2/n$ is indeed found for the complexes $Ni(terpy)_2(NO_3)_2 \cdot 3H_2O$[12,16] and $Co(terpy)_2I_2 \cdot 2H_2O$.[13] For the former compound only the substructure could be solved. The deviation of the superstructure from $P4_2/n$ is very small and presumably induced by the anions and the water molecules. The geometry of the NiN_6 polyhedra reflects the extent of the ligand strain, which induces a tetragonal compression of $\bar{4}$ symmetry. The value for the radial distortion parameter is much smaller (0.14_5 Å) than the one that characterizes the static limit in $Cu(terpy)_2(NO_3)_2$ (≈0.35 Å) (Table IV).

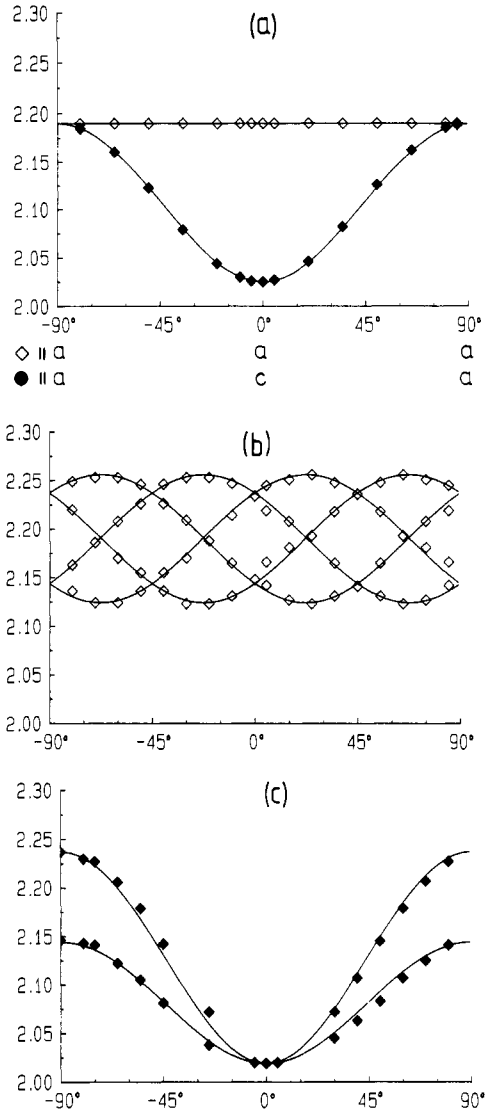

Figure 7. Angular dependencies of the g values of Cu(II)-doped $Zn(terpy)_2(PF_6)_2$ single crystals in the (001) plane (◇) and in the (010) [or (100)] plane (◆): 298 K (a) and 4.2 K (b, c).

In the Co^{2+} complex ρ is larger, because Co^{2+} is involved in a temperature-dependent high-spin–low-spin equilibrium; the low-spin character increases when the temperature is lowered, and this enlarges the Jahn–Teller contribution to the radial distortion parameter.[14] Below 80 K the g tensor becomes orthohombic, with the same angular dependence as observed for $Cu(terpy)_2(NO_3)_2$. Apparently the ligand strain has a more significant influence on the geometry in comparison to the Jahn–Teller coupling than in the case of Cu^{2+}, as is documented by the rather small ρ value and the much larger deviation of the angular parameter from φ = 120° (Table IV, 4.2 K data).[14] Thus, we may state that a phase transition to a new unit cell with the space group $I4_1/a$ accompanies the freezing mechanism from the dynamic to the static Jahn–Teller effect (antiferrodistortive order) if the high-temperature phase belongs to the space group $P4_2/n$. The continuous nature of the phase transition is expected, because $I4_1/a$ is a (maximal nonisomorphic) subgroup of $P4_2/n$.[17]

The high-temperature phase of $Cu(terpy)_2(PF_6)_2$ (space group $P\bar{4}2_1c$) differs from the one with space group $P4_2/n$ only by different orientations of the two CuN_6 polyhedra in the (001) planes with respect to each other (Figure 6a,b). While the directions of the projections of the four longer Cu(Ni)–N bonds onto the (001) plane are parallel for the two CuN_6 entities in $P4_2/n$, they are connected by a c glide plane in $P\bar{4}2_1c$, thus introducing a canting angle between the two polyhedra.[7] The only

(16) Reinen, D. In *Biological and Inorganic Copper Chemistry*; Karlin, K. D., Zubieta, J., Eds.; Adenine Press: New York, 1985; p 247.

(17) *International Tables for X-ray Crystallography*; Reidel: Dordrecht, Holland, 1983; Vol. A.

space group that properly accounts for the single-crystal EPR data of the low-temperature phase and that is in accord with a group–subgroup relation[17] is $I\bar{4}$. The Cu^{2+} positions 8e on a 2-fold axis in $I4_1/a$ are split into two positions 4e and 4f. The two antiferrodistortive pairs of magnetically inequivalent sublattices A (0, 0, $\bar{z}$), A' ($^1/_2$, $^1/_2$, $^1/_2 + z$) ($z \geq {}^1/_4$) and B (0, $^1/_2$, z), B' ($^1/_2$, 0, $\bar{z}$) ($z \geq 0$) are identical in $I4_1/a$ (($A = B'$ and $A' = B$; Figure 6b) but independent and differently oriented in $I\bar{4}$ (Figure 6a), in accord with the EPR data discussed above. The coordinates of the $I\bar{4}$ cell are transformed into those of the smaller $P\bar{4}2_1c$ unit cell also by matrix (M1), if the z parameters in 4e and 4f are fixed at $-^1/_4$ and 0, respectively.

EPR powder data are also available for $Cu(terpy)_2X_2 \cdot nH_2O$ with X = ClO_4, n = 1 and X = Br, n = 1.[15,16] The tetragonal **g** tensor at 298 K becomes orthorhombic at lower temperatures. The ρ and φ parameters (Table IV) derived from the g values and ligand field transitions at 4.2 K, assuming the same a_z and $\bar{a}$ spacings as for the nitrate, are in the expected range. It remains open to question whether the high- and low-temperature phases have the space groups $P4_2/n$ and $I4_1/a$ or $P\bar{4}2_1c$ and $I\bar{4}$.

A third alternative structure for pseudooctahedral $Cu(terpy)_2X_2 \cdot nH_2O$ compounds is that found for the bromide with three water molecules. It has the same space group $P\bar{1}$ as that reported earlier for the corresponding Co^{2+} compound.[9] In contrast to the Co^{2+} complex with $\varphi = 180°$ for the local CoN_6 geometry, a small orthorhombic symmetry component is found for the CuN_6 polyhedron (Figure 3, Table IV), in accord with the **g**-tensor components: $g_z = 2.03_0$, $g_y = 2.15_0$, $g_x = 2.20_0$. The **g** tensor at 170 K with $g_z = 2.02_9$, $g_y = 2.122$, and $g_x = 2.22_0$ indicates a more pronounced orthorhombicity of the Cu–N spacings. It is to be expected that the static limit at 4.2 K will correspond to a radial distortion parameter ρ in the range of those observed for the other Cu^{2+} compounds (Table IV). Though the single-crystal EPR experiments could not be extended to lower temperatures because the complex looses water rapidly, it is evident that only one signal is observed. This is in accord with the ferrodistortive order in this compound, in contrast to the other cases discussed before (Figure 6c). The analogous Co^{2+} complex is fully dynamic at 298 K, which is apparently due to a slight admixture of high-spin character to the low-spin ground state. Apparently the transition from the dynamic to the static Jahn–Teller distortion occurs continuously and without a change of the space group $P\bar{1}$. The coordinates of the triclinic cell (x, y, z) can be transformed into those of a cell with $Z = 8$ (x', y', z') [$a' = 13.46$ Å, $b' = 12.21$ Å, $c' = 39.96$ Å; $\alpha = 82.9°$, $\beta = 89.2°$, $\gamma = 82.5°$] by the matrix equation (M2).[12] The new cell (Figure 6c) can be directly compared with

$$\begin{pmatrix} 0 & ½ & ½ \\ 0 & ½ & -½ \\ ½ & 0 & 0 \end{pmatrix} \qquad \text{(M2)}$$

that for $Cu(terpy)_2(NO_3)_2$ [$a = 12.476$ (6) Å, $c = 36.284$ (13) Å][11] (Figure 6b), if the origin is additionally shifted by 0, $-^1/_4$, $+^1/_8$. In the pseudotetragonal cell there are again layers of Cu^{2+} ion with positional parameters even nearer to 0, $^1/_4$, $^1/_2$ and $^3/_4$ than those for the nitrate. The layers are shifted with respect to each other in particular in the b' direction (by about $\pm 0.13_5$ along the y coordinate), however, and the CuN_6 polyhedra are ferrodistortively ordered, as stated above already. The c' constant is larger by about 3.7 Å than that for the nitrate complex, due to the water layers perpendicular to this direction (Figure 3). The symmetry correlation between the triclinic $P\bar{1}$ and the tetragonal $I4_1/a$ unit cells has recently been analyzed in a similar way by White et al.[18]

Properties of the "tpt" Complexes. By working in ethanol solutions, using a convenient Cu:tpt molar ratio and noncoordinating counterions, we have been able to isolate solids with $Cu(tpt)_2X_2 \cdot nH_2O$ stoichiometry. The ethanolic medium inhibits the well-known Cu(II)-promoted tpt hydrolysis[4,5] and allows one to easily separate those compounds due to their poor solubility in this medium. Up to now, attempts to grow single crystals have failed, however. The analytical data (Table I) are in agreement with the proposed compositions, and IR absorptions at about 1710 cm^{-1}, which could be associated with the strong absorption of an imide group from hydrolized derivatives,[4,5] are never observed. All compounds evolve water at very low temperatures (70–95 °C). This fact, together with the shape and position of the ν_s (O–H) bands (≈3400 cm^{-1}, broadened) and the lack of bands assignable to Cu–OH_2 bonds, is indicative of noncoordinated water molecules and of moderate- to low-intensity hydrogen bonds.[19] On the other hand, there is no indication in the IR spectra for coordination of the anions.[20] All the solids are crystalline powders, and from their nearly identical X-ray diffraction patterns, the structural equivalence of the three monohydrated derivatives can be suggested. The patterns can be indexed on the basis of a tetragonal unit cell, whereas those corresponding to the hexafluorophosphate salt can be indexed to an orthorhombic unit cell, with the parameters given in Table I.

The electronic reflectance spectra of all derivatives show two broad bands with maxima around 6500 and 14000 cm^{-1}. We have assigned them by following the arguments and MO calculations for the $Cu(terpy)_2^{2+}$ complex in ref 15. The D_{2d} point group of a thermally averaged entity is reduced to C_{2v} if the Jahn–Teller distortion becomes static. If the long axis extends along x, a term sequence $_a{}^2A_1$ (≈$z^2 - y^2$), $_b{}^2A_1$ (≈x^2), $^2B_2$ (yz), $^2B_1$ (xz), and $^2A_2$ (xy) is expected (Figure 2). The deviation of the Cu–N bonds from the x and y axes (≈ 13°), however, changes the sequence for the $^2T_2$-split states to $^2A_2$, $^2B_2$, and $^2B_1$.[15] The assignment of the two bands to the symmetry-allowed transitions $_a{}^2A_1 \rightarrow {}_b{}^2A_1$ and $_a{}^2A_1 \rightarrow {}^2B_2$ (yz), $^2B_1$ (xz), respectively, is now straightforward. The $^2B_2$ and $^2B_1$ states are closely spaced[15] and not resolved in the reflectance spectrum. The derived Jahn–Teller stabilization energies and octahedral ligand field parameters are listed in Table I. The values are similar to those reported in the literature for related CuN_6 polyhedra.[3,8,15]

EPR Results and Bonding Parameters. The full set of EPR data for the complexes studied in this work are listed in Table V. The φ values have been estimated from the well-known expressions relating the g_i values ($i = x, y, z$) and the φ and the orbital contributions u_i but assuming $u_x = u_y = u_z = u$.[3] g_z remains practically unchanged with decreasing temperature and has nearly the same value for all investigated compounds: $g_z \approx 2.025$ (5) and obviously reflects the strain-induced compression. Moreover, all compounds exhibit nearly identical "fluxional" behavior, as is indicated by the variation of the g_x and g_y values with the temperature. The static limit is characterized by an angular parameter $\gamma = 140$ (6)°.

Concerning the $Cu(terpy)_2(PF_6)_2$ compound, an interesting feature of the EPR spectra at 4.2 K may be mentioned. Depending on the experimental conditions (microwave power in particular), a shift of the resonance fields is observed, which may be due to the presence of very weak internal magnetic fields arising from magnetic interactions between the copper polyhedra. Phenomena of this kind are frequently observed in weak ferromagnets such as K_2CuF_4 with a similar antiferrodistortive order.[1]

The tpt complexes, for which structural data are not available, apparently behave similar to the terpy complexes. In particular, the PF_6^- salt shows the inverse axial EPR spectrum at room temperature due to a "planar dynamics" of the CuN_6 polyhedra. The "freezing-in" process, however, seems to start at higher temperatures because the three g components are separated already at 77 K. It should be noted that g_z and g_x hyperfine structures are observed in the powder spectra, which is not the case for the terpy salt (Figures 5 and 8). It is presumably due to larger Cu–Cu separations because of the greater volume of the

(18) Figgis, B. N.; Kucharski, E. S.; White, A. H. *Aust. J. Chem.* **1983**, *36*, 1537.

(19) Falk, M.; Knop, D. In *Water: a Comprehensive Treatise*; Frank, F., Ed.; Plenum Press: New York, 1973; Vol. 2, Chapter 2.

(20) Nakamoto, K. *Infrared and Raman Spectra of Inorganic and Coordination Compounds*, 4th ed.; J. Wiley and Sons: New York, 1986; p 130.

Table V. EPR Data for the Studied Complexes[a]

compd	T, K	g_x	g_y	g_z	y	φ, deg	$\lvert A_x\rvert$, 10^{-4} cm^{-1}	$\lvert A_z\rvert$, 10^{-4} cm^{-1}	κ	α
$Cu(terpy)_2(PF_6)_2$[b,c]	298	2.191		2.023	0.032	180				
		(2.190)		(2.026)	(0.032)	(180)		(71)		
	77	(2.230)	(2.160)	(2.020)	(0.034)	(161)		(71)		
	4.2	≃2.26	2.129	2.020	0.036	*146*	126	71	0.23	0.92
		(2.256)	(2.123)	(2.020)	(0.034)	(*146*)	(126)	(71)	(0.23)	(0.92)
$Cu(terpy)_2Br_2\cdot 3H_2O$[b]	298	2.199	2.150	2.030	0.030	165				
	170	2.219	2.122	2.027	0.030	150				
$Cu(tpt)_2(PF_6)_2\cdot 3H_2O$	298	2.191		2.021	0.032	180		≃75		
		(2.230)	(2.150)	(2.020)	(0.034)	(158)		(≃75)		
	77	2.238	2.150	2.020	0.034	157		≃75		
		(2.260)	(2.120)	(2.020)	(0.035)	(145)	(127)	(75)		
	4.2	2.258	2.118	2.021	0.034	*144*	124	75	0.22	0.92
		(≃2.26)	(≃2.21)	(2.02)	(0.035)	(*141*)	(130)	(75)	(0.22)	(0.92)
$Cu(tpt)_2X_2\cdot H_2O$ (X = ClO_4, Br)	298	2.22	2.15	2.03	0.032	159				
		(2.22)	(2.16)	(2.02)	(0.033)	(162)		(71)		
	77	2.25	2.11	2.03	0.033	141				
		(2.25)	(2.11)	(2.02)	(0.033)	(143)	(131)	(71)		
	4.2	2.26	2.10	2.03	0.034	*137*				
		(2.26)	(2.10)	(2.02)	(0.034)	(*139*)	(132)	(71)	(0.20)	(0.93)
$Cu(bpca)_2\cdot H_2O$	298	2.234	2.108	2.027	0.031	143				
		(2.238)	(2.118)	(2.025)	(0.032)	(146)	(118)	(63)		
	77	2.247	2.087	2.032	0.032	134				
		(2.252)	(2.093)	(2.030)	(0.033)	(136)	(142)	(57)		
	4.2	2.250	2.083	2.031	0.032	*133*				
		(2.256)	(2.089)	(2.030)	(0.033)	(*135*)	(150)	(57)	(0.24)	(0.94)

[a] Values corresponding to Cu(II) doped into Zn(II) compounds are given in parentheses. Italicized data represent the static limit. The molecular z, y, and x coordinates correspond, respectively, to the short, intermediate, and long bond lengths of the distorted CuN_6 octahedra. [b] EPR single-crystal data. [c] The powder spectra yield practically the same g values, but the hyperfine structure is less resolved.

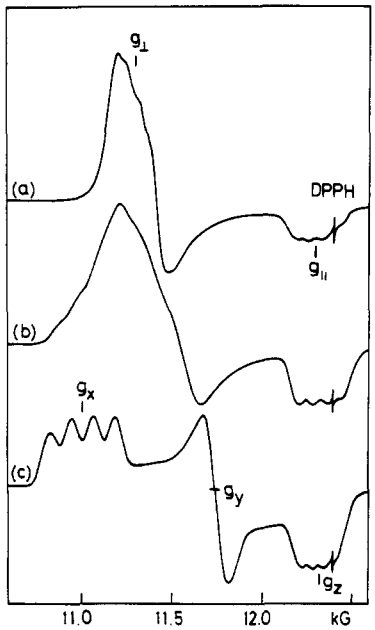

Figure 8. EPR powder spectra (35 GHz) of $Cu(tpt)_2(PF_6)_2\cdot 3H_2O$ at room temperature (a), 77 K (b), and 4.2 K (c).

tpt ligand and the presence of three water molecules of crystallization. The g values for pure and doped compounds are practically identical except for the tpt–PF_6^- derivative, where the freezing-in occurs at higher temperatures in doped than in the pure compound. Possibly, lattice defects in the poorly crystallized doped samples are responsible for this behavior, stabilizing one of the lower minima with respect to the other (Figure 1).

Finally, for comparative purposes, we have recorded the Q-band EPR spectra on pure and Cu(II) doped into Zn(II) powder samples of $Cu(bpca)_2\cdot H_2O$. The unit cell of the Cu^{2+} compound contains four isolated orthorhombically distorted CuN_6 octahedra.[8] The two magnetically inequivalent polyhedra span two sublattices with a canting angle of ≈40°, nearly intermediate between the ferrodistortive (0°) and antiferrodistortive (90°) limiting situations. This cooperative order pattern imposes an orthorhombic strain on the ground-state potential surface additionally to the rigid ligand effect, which eventually lowers one of the two lower minima with respect to the other. The observation of nearly equal g values in comparison with the doped complexes indicates, however, that the cooperative strain component is as negligibly small as for the other complexes in Table V. Similarly to $Cu(terpy)_2(NO_3)_2$, the static limit is maintained up to 77 K, in contrast to the other investigated complexes.

The metal hyperfine components in a pseudooctahedral copper(II) complex with orthorhombic symmetry can be expressed by the equations

$$A_x = P\left\{[-\kappa + {}^2/_7(\cos\varphi - \sqrt{3}\sin\varphi)]\alpha^2 + \frac{\sqrt{3}(g_z - g_0)\sin\varphi}{14(1+\cos\varphi)} - \frac{(g_y - g_0)(3 + 2\sqrt{3}\sin\varphi)}{14(2\cos\varphi - 1)} + (g_x - g_0)\right\}$$

$$A_y = P\left\{[-\kappa + {}^2/_7(\cos\varphi - \sqrt{3}\sin\varphi)]\alpha^2 + \frac{\sqrt{3}(g_z - g_0)\sin\varphi}{14(1+\cos\varphi)} - \frac{(g_x - g_0)(3 - 2\sqrt{3}\sin\varphi)}{14(2\cos\varphi - 1)} + (g_y - g_0)\right\}$$

$$A_z = P\left[(-\kappa - {}^4/_7\cos\varphi)\alpha^2 + \frac{(g_x - g_0)(3 - 2\sqrt{3}\sin\varphi)}{14(2\cos\varphi - 1)} + \frac{(g_y - g_0)(3 + 2\sqrt{3}\sin\varphi)}{14(2\cos\varphi - 1)} + (g_z - g_0)\right] \quad (2)$$

where α is the mixing coefficient of the Cu^{2+} orbital in the ground-state MO of $^2A_{1g}$ symmetry and $P\kappa$ is the isotropic contribution to the hyperfine coupling (Fermi contact term). κ is considered to be dominated by the polarization of the core s electrons by the unpaired d electrons and has been calculated to be 0.43 for the free Cu^{2+} ion. The generally assumed value for the scaling factor P is 0.036 cm^{-1}.[21,22] These values nicely re-

(21) Abragam, A.; Price, M. H. L. *Proc. R. Soc. London, A* **1955**, *230*, 169.

produce the hyperfine parameters of Cu(II) complexes with $d_{x^2-y^2}$ ($d_{z^2-x^2}$, $d_{y^2-z^2}$) ground states. However, the hyperfine parameters found in the complexes under consideration (Table V) are not in accord with $\kappa = 0.43$. From the experimental A_z and A_x values the κ and α parameters of Table V are estimated if the calculated φ angles are used and A_z and A_x have positive and negative signs, respectively. The depression of κ is directly correlated with a participation of the metal 4s orbital in the ground state, which is expected to have an effect opposite in sign to that of the polarized core electrons.[22]

A critical review of the calculated φ angles (140 ± 6°), κ values (0.22 ± 0.02), and α coefficients (0.93 ± 0.01) for the static limits listed in Table V imposes the need of small adjustments. The ligand field spectra show two broad transitions at 6500 ± 400 and 13 900 ± 100 cm^{-1} (Tables I and II), which can be assigned to the three symmetry-allowed transitons in he C_{2v} point group: $_a{}^2A_1$ ($\approx z^2 - y^2$) → $_b{}^2A_1$ ($\approx x^2$) and → $^2B_2$ (yz), $^2B_1$ (xz) (see previous section). The symmetry-forbidden transition $_a{}^2A_1 \rightarrow {}^2A_2$ (xy) is not observed but calculated to occur at about 13 000 cm^{-1}. This would imply a nonequivalence of the orbital contributions with $u_z > u_x \approx u_y$—in contrast to our earlier assumption of identical u_l contributions—and raises the angular parameters φ by about 5°, which on the other hand changes κ to 0.24 ± 0.02 and lowers α by about 0.01. An additional slight decrease of α has to be taken into account, because the equatorial Cu-N bond lengths deviate from the molecular x and y directions (Figure 2). The resulting α values of 0.91 (1) are larger than those that have been reported for the CuN_6 polyhedra in $Cu(TACN)_2^{2+}$ (TACN = 1,4,7-triazacyclononane)[24] and in hexanitro complexes[25] with $d_{x^2-y^2}$ ($d_{z^2-y^2}$) ground states ($\alpha = 0.87$). Possibly this is partly due to the $d_x{}^2$ admixture to the $d_{z^2-y^2}$ ground state, which is about 10 ± 3% for the compounds of Table V. Indeed the CoN_6 polyhedra in low-spin $Co(TACN)_2^{2+}$, which exhibit Jahn-Teller effects of comparable strength to that of Cu^{2+} but possess $d_z{}^2$ ($d_x{}^2$) ground states, have much larger α coefficients ($\alpha = 0.93$) than those of the just mentioned CuN_6 polyhedra in the same coordination. The calculated κ value (≈0.24) allows one to estimate the fractional occupancy of the 4s orbital by the unpaired electron.[23,26] The amount of 2.8% reasonably compares with the 4.5% calculated for the just mentioned $Co(TACN)_2^{2+}$ complex.[24]

Acknowledgment. We wish to acknowledge financial support by the Comision Interministerial de Ciencia y Tecnologia and the Fonds der Chemischen Industrie. The receipt of a research fellowship for a postdoctoral stay in Marburg from the Generalitat Valenciana is gratefully acknowledged by J.-V.F.

Supplementary Material Available: Table SI (complete crystallographic data) and Table SII (anisotropic thermal parameters of all atoms besides hydrogen; atomic positions and isotropic thermal parameters for hydrogen) (4 pages); Table SIII (observed and calculated structure factors) (7 pages). Ordering information is given on any current masthead page.

(22) McGarvey, B. R. *J. Phys. Chem.* **1967**, *71*, 51.
(23) Hitchman, M. A.; McDonald, R. G.; Reinen, D. *Inorg. Chem.* **1986**, *25*, 519.
(24) Reinen, D.; Ozarowski, A.; Jakob, B.; Pebler, J.; Stratemeier, H.; Wieghardt, K.; Tolksdorf, I. *Inorg. Chem.* **1987**, *26*, 4010.
(25) Ozarowski, A.; Reinen, D. *Inorg. Chem.* **1985**, *24*, 3860.
(26) Morton, J. R.; Preston, K. F. *J. Magn. Reson.* **1978**, *30*, 577.

Contribution from the Department of Inorganic Chemistry, University of Barcelona, Diagonal 647, 08028-Barcelona, Spain, Laboratoire de Chimie Inorganique, URA No. 420, Université de Paris-Sud, 91405 Orsay, France, and Laboratoire de Chimie de Coordination du CNRS, UP No. 8241, 205 route de Narbonne, 31077 Toulouse, France

Structure and Magnetic and Spectroscopic Properties of a $Ni^{II}Cu^{II}Ni^{II}$ Trinuclear Species

Juan Ribas,*[1a] Carmen Diaz,[1a] Ramon Costa,[1a] Yves Journaux,[1b] Corine Mathoniere,[1b] Olivier Kahn,*[1b] and Alain Gleizes[1c]

Received September 6, 1989

The two compounds of formula $\{[Ni(bapa)(H_2O)]_2Cu(pba)\}(ClO_4)_2$ and $[Ni(bapa)(H_2O)Cu(pba)]\cdot 2H_2O$, hereafter abbreviated as [NiCuNi] and [NiCu], respectively, have been synthesized. bapa is bis(3-aminopropyl), and pba is 1,3-propylenebis(oxamato). The crystal structure of [NiCuNi] has been solved. It crystallizes in the orthorhombic system, space group $Pna2_1$, with a = 9.826 (2) Å, b = 12.793 (1) Å, c = 27.266 (3) Å, and Z = 4. The structure consists of $Ni^{II}Cu^{II}Ni^{II}$ trinuclear cations and noncoordinated perchlorate anions. The nickel atoms are in a distorted octahedral environment, and the copper atom is in an environment markedly distorted from square planar to tetrahedral. The central copper atom is bridged to the terminal nickel atoms by oxamato groups with Cu···Ni separations of 5.305 (2) and 5.326 (2) Å. The magnetic properties of both compounds have been investigated. The $\chi_M T$ versus T plot (χ_M is the molar magnetic susceptibility and T the temperature) for [NiCuNi] exhibits the minimum characteristic for this kind of polymetallic species with an irregular spin state structure. The Ni(II)-Cu(II) isotropic interaction parameter was found to be $J = -90.3$ cm^{-1} ($H = -JS_{Ni} \cdot S_{Cu}$). The powder EPR spectrum at 10 K is poorly resolved. It shows a broad signal corresponding to the envelope of the two Kramers doublets arising from the spin-quartet ground state. The $\chi_M T$ versus T plot for [NiCu] is typical of an antiferromagnetically coupled pair with a spin-doublet ground state and a doublet-quartet energy gap equal to $3J/2 = -141.9$ cm^{-1}. The electronic spectra of [NiCuNi] has also been investigated. It shows a triplet → singlet spin-forbidden transition associated with the nickel(II) ion and activated by an exchange mechanism.

Introduction

We have recently pointed out that it was possible to stabilize a state of high-spin multiplicity in a polymetallic entity without imposing ferromagnetic interactions between nearest neighbor magnetic centers.[2,3] The strategy for this consists of aligning two high local spins along the same direction owing to antiferromagnetic interactions with a small local spin located between them. The basic scheme for describing the ground state of a trinuclear species of this kind is

(1) (a) University of Barcelona. (b) Université de Paris-Sud. (c) Laboratoire de Chimie de Coordination du CNRS. Present address: ENSCT, URA No. 445, 118 route de Narbonne, 31077 Toulouse, France.
(2) Pei, Y.; Journaux, Y.; Kahn, O. *Inorg. Chem.* **1988**, *27*, 399.
(3) Kahn, O. *Struct. Bonding (Berlin)* **1987**, *68*, 89.
(4) Verdaguer, M.; Julve, M.; Michalowicz, A.; Kahn, O. *Inorg. Chem.* **1983**, *22*, 2624.
(5) Drillon, M.; Gianduzzo, J. C.; Georges, R. *Phys. Lett.* **1983**, *96A*, 413.
(6) Gleizes, A.; Verdaguer, M. *J. Am. Chem. Soc.* **1984**, *106*, 3727.
(7) Beltran, D.; Escriva, E.; Drillon, M. *J. Chem. Soc., Faraday Trans. 2* **1982**, *78*, 1773.
(8) Coronado, E.; Drillon, M.; Fuertes, A.; Beltran, D.; Mosset, A.; Galy, J. *J. Am. Chem. Soc.* **1986**, *108*, 900.
(9) Pei, Y.; Verdaguer, M.; Kahn, O.; Sletten, J.; Renard, J. P. *Inorg. Chem.* **1987**, *26*, 138.

0020-1669/90/1329-2042$02.50/0